JACS
JOURNAL OF THE AMERICAN CHEMICAL SOCIETY
Article
pubs.acs.org/JACS

In Situ Analysis of 8-Oxo-7,8-dihydro-2′-deoxyguanosine Oxidation Reveals Sequence- and Agent-Specific Damage Spectra

Kok Seong Lim,*[,†] Liang Cui,[†,⊥] Koli Taghizadeh,[§] John S. Wishnok,[†,§] Wan Chan,[†,∥] Michael S. DeMott,[†] I. Ramesh Babu,[†] Steven R. Tannenbaum,[†,‡] and Peter C. Dedon*[,†,§]

Departments of [†]Biological Engineering and [‡]Chemistry, and [§]Center for Environmental Health Science, Massachusetts Institute of Technology, Cambridge, Massachusetts 02139, United States

Supporting Information

ABSTRACT: Guanine is a major target for oxidation in DNA, with 8-oxo-7,8-dihydro-2′-deoxyguanosine (8-oxodG) as a major product. 8-oxodG is itself significantly more susceptible to oxidation than guanine, with the resulting damage consisting of more than 10 different products. This complexity has hampered efforts to understand the determinants of biologically relevant DNA oxidation chemistry. To address this problem, we have developed a high mass accuracy mass spectrometric method to quantify oxidation products arising site specifically in DNA. We applied this method to quantify the role of sequence context in defining the spectrum of damage products arising from oxidation of 8-oxodG by two oxidants: nitrosoperoxycarbonate ($ONOOCO_2^-$), a macrophage-derived chemical mediator of inflammation, and the classical one-electron oxidant, riboflavin-mediated photooxidation. The results reveal the predominance of dehydroguanidinohydantoin (DGh) in 8-oxodG oxidation by both oxidants. While the relative quantities of 8-oxodG oxidation products arising from $ONOOCO_2^-$ did not vary as a function of sequence context, products of riboflavin-mediated photooxidation of 8-oxodG were highly sequence dependent. Several of the 8-oxodG oxidation products underwent hydrolytic conversion to new products with half-lives of 2−7 h. The results have implications for understanding the chemistry of DNA oxidation and the biological response to the damage, with DNA damage recognition and repair systems faced with a complex and dynamic set of damage targets.

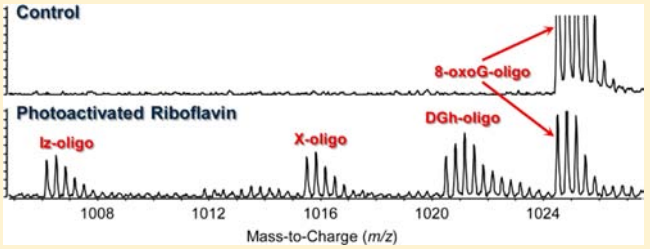

INTRODUCTION

A growing body of evidence points to a strong influence of local DNA structure and sequence context on the chemistry and location of DNA damage in the genome.[1−4] This is most clearly illustrated for the location of DNA damage caused by oxidation.[5,6] Due to its low reduction potential, guanine (G) is the most readily oxidized site in DNA, with one-electron oxidants, such as photoactivated riboflavin causing G oxidation that leads to charge migration to Gs in sequence contexts that confer the lowest ionization potential, such as the 5′ end of runs of G.[7−10] However, the biologically relevant oxidant, nitrosoperoxycarbonate ($ONOOCO_2^-$), which arises from macrophage-derived nitric oxide (NO) and superoxide ($O_2^{\bullet-}$), preferentially oxidizes Gs with the highest ionization potential (IP),[11,12] while charge migration plays a relatively minor role in determining the location of G oxidation by hydroxyl radical.[13] These results point to oxidant-specific determinants of the location of G oxidation, in addition to the sequence-context effects on G oxidation.

While there is strong mechanistic evidence for sequence determinants of damage localization, there is far less known about the effect of sequence context on the chemistry of DNA oxidation. The complexity of G oxidation chemistry is illustrated in Figure 1 for a major product of G oxidation: 8-oxo-7,8-dihydro-2′-deoxyguanosine (8-oxodG). 8-OxodG is significantly more reactive than guanine itself[14−17] and is oxidized to form a variety of damage products, such as dehydroguanidinohydantoin (DGh), trioxo-[1,3,5]-triazinane-1-carboxamidine (CAC), cyanuric acid (CA), *N*-nitro-dehydroguanidinohydantoin (NO_2-DGh), parabanic acid (PA), 5-guanidinohydantoin (Gh), 4-hydroxy-2,5-dioxo-imidazolidine-4-carboxylic acid (HICA), oxaluric acid (OA), imidazolone (Iz), oxazolone (Ox), and 2-imino-5,5′-spirodihydantoin (Sp) (Figure 1).[18−20] Several groups have used chemically nonspecific and semiquantitative techniques to show sequence-dependent variation in classes of oxidatively damaged nucleobases in DNA (e.g., lesions sensitive to hot piperidine versus DNA glycosylase enzymes).[11,21] However, the relative insensitivity and nonspecific nature of these approaches limit the mechanistic information needed for understanding the role of DNA damage location and chemistry in mutagenesis.

In the present study, we have approached the problem of sequence context effects on DNA oxidation chemistry by developing a method to identify and quantify specific 8-oxodG oxidation products *in situ* in intact oligodeoxyribonucleotides using liquid chromatography-coupled, high mass accuracy quadrupole-time-of-flight mass spectrometry (LC-QTOF).

Received: July 31, 2012
Published: October 11, 2012

dx.doi.org/10.1021/ja307525h | J. Am. Chem. Soc. 2012, 134, 18053−18064

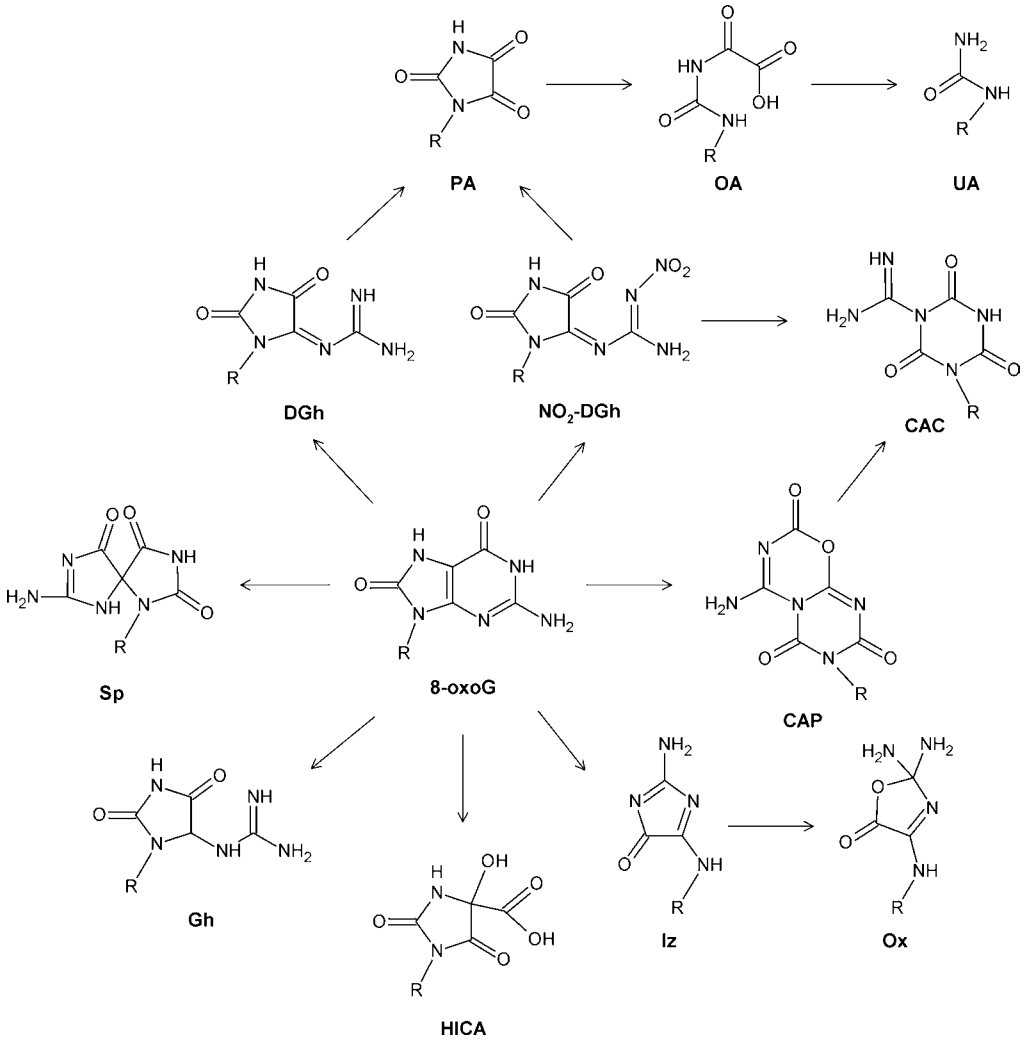

Figure 1. Chemistry of 8-oxodG oxidation.

This approach revealed significant effects of both sequence context and the identity of the oxidant on the spectrum of DNA oxidation products as well as the discovery of a novel DNA oxidation product and transformation of DNA lesions on a biologically relevant time scale. The results have implications for understanding the chemistry of DNA oxidation and the biological response to the damage.

EXPERIMENTAL METHODS

Chemicals. All chemicals and reagents were of the highest purity available and were used without further purification. Ammonium acetate, sodium chloride, and tris(hydroxymethyl)aminomethane were purchased from American Bioanalytical (Natick, MA); EDTA, potassium phosphate, sodium bicarbonate from Mallinckrodt (Paris, KY); acetonitrile from EMD Chemicals (Gibbstown, NJ); peroxynitrite from Cayman Chemical (Ann Arbor, MI; peroxynitrite concentration was determined spectrophotometrically in 0.3 M NaOH with A_{302} = 1670 M^{-1} cm^{-1}); and riboflavin from Sigma (St. Louis, MO). Uniformly [^{13}C,^{15}N]-labeled dG (^{13}C and ^{15}N > 98%) was obtained from Cambridge Isotope Laboratories (Andover, MA). Deionized water was purified with a Milli-Q system (Millipore Corporation, Bedford, MA) and autoclaved prior to use in all experiments. The oligodeoxyribonucleotides used in these experiments were purchased from the Midland Certified Reagent Company, Inc. (Midland, TX).[22] Double-stranded oligodeoxyribonucleotides were prepared as described previously.[22]

Instrumental Analyses. UV−vis measurements were made on an HP8452 diode-array spectrophotometer (Agilent Technologies). HPLC analyses were carried out on an Agilent 1100 HPLC system with binary pumps, a degasser, and an autoinjector. Quantitative LC-MS/MS analyses were conducted on an Agilent 1100 HPLC pump system interfaced with an Agilent 6430 triple quadrupole mass spectrometer. Electrospray ionization (ESI)-MS experiments for isotopic purity and structural confirmation were performed on an Agilent MSD-TOF mass spectrometer.

Synthesis and Purification of Standards. *Spiroiminodihydantoin and [^{13}C,^{15}N]-Labeled Spiroiminodihydantoin.* A mixture of 3.0 mg of rose bengal and 5 mg of dG or the uniformly [^{13}C,^{15}N]-labeled dG in 10 mL of water was adjusted to pH of 9−10 by the addition of 6 μL of 5 M NaOH. The reaction mixture was incubated for 4 h with stirring and irradiated by a 100 W incandescent light bulb positioned at a distance of 6−8 cm. After the incubation, the pH of the solution was adjusted to ∼2 by the dropwise addition of 1 M HCl. The red rose bengal precipitate was removed by filtration with a 0.2 μm syringe filter. Then the pH of filtered solution was adjusted to 7−8 by addition of 5 M NaOH. The filtrate was applied to a Waters Sep-pak C_{18} cartridge (Waters, Milford, MA), which had been preconditioned with 3 mL of methanol, followed by 3 mL of water. The SPE column was washed with 3 mL of 2% methanol, and the eluant was purified by HPLC using a Luna-amino column (250 × 4.6 mm, 5 μm; Phenomenex, Torrance, CA). The mobile phase was 20 mM ammonium formate (A) and acetonitrile (B) as an isocratic mixture of 80% A and 20% B at a flow rate of 1.0 mL/min. The retention times of the two diastereoisomers of Sp were 12 and 14 min. The eluted

dx.doi.org/10.1021/ja307525h | J. Am. Chem. Soc. 2012, 134, 18053−18064

Table 1. Mass-to-Charge Ratios of Oligodeoxyribonucleotides Containing 8-oxodG in Different Sequence Contexts[a]

name	strand	sequence	mol wt[b]	m/z[c] measured(n = 3)	m/z[c] calculated
AOC	8-oxodG	CAGAAA**O**CCC	3020.557	1005.844 ± 0.001	1005.844
	complement	GGGCTTTCTG	3048.527	1015.168 ± 0.001	1015.168
COA	8-oxodG	CAGAA**CO**ACC	3020.557	1005.845 ± 0.000	1005.844
	complement	GGTCGTTCTG	3048.527	1015.168 ± 0.001	1015.168
GOG	8-oxodG	CAGAA**GO**GCC	3076.558	1024.512 ± 0.002	1024.511
	complement	GGCCCTTCTG	2993.521	996.833 ± 0.000	996.832
AOG	8-oxodG	CAGAAA**OG**CC	3060.563	1019.180 ± 0.001	1019.180
	complement	GGCCTTTCTG	3008.521	1001.833 ± 0.001	1001.832
COT	8-oxodG	CAGAA**COT**CC	3011.545	1002.840 ± 0.002	1002.840
	complement	GGACGTTCTG	3057.539	1018.172 ± 0.001	1018.171
TOC	8-oxodG	CAGAA**TO**CCC	3011.545	1002.840 ± 0.000	1002.840
	complement	GGGCATTCTG	3057.539	1018.172 ± 0.000	1018.171
AGC	dG	CAGAAA**G**CCC	3004.561	1000.512 ± 0.002	1000.512
	complement	GGGCTTTCTG	3048.527	1015.168 ± 0.001	1015.168
CGA	dG	CAGAA**CG**ACC	3004.561	1000.511 ± 0.001	1000.512
	complement	GGTCGTTCTG	3048.527	1015.167 ± 0.000	1015.168
GGG	dG	CAGAA**GGG**CC	3060.562	1019.179 ± 0.001	1019.179
	complement	GGCCCTTCTG	2993.521	996.833 ± 0.000	996.832

[a]The position of 8-oxodG is denoted by "O". [b]Molecular weight based upon Mongo Oligo Mass Calculator, v2.06. [c]Based on the ion with −3 charge state in negative ion mode with at least 6 ppm accuracy.

fractions containing Sp were collected, and their concentration was measured by UV absorbance at 230 nm (ε = 10 500 M^{-1} cm^{-1}).

Guanidinohydantoin and [^{13}C,^{15}N]-Labeled Guanidinohydantoin. A mixture of 3 mg of rose bengal, 7 mg of dG or the uniformly [^{13}C,^{15}N]-labeled dG, and 10 mL of 37.5 mM potassium phosphate (pH 4.5) was incubated at 4 °C for 3 h while stirring and irradiated by a 100 W light positioned at a distance of 6−8 cm. After the incubation, the pH of the solution was adjusted to about 2 by the addition of 1 M HCl dropwise. The red rose Bengal precipitate was filtered with a 0.2 μm syringe filter. Then the pH of filtered solution was adjusted back to 4 by adding 5 M NaOH. The filtrate was applied to a Waters Sep-pak C_{18} cartridge (Waters), which had been preconditioned by 3 mL of methanol, followed by 3 mL water. The SPE column was washed with 3 mL of 2% methanol, and the eluant was purified by HPLC using a Hypercarb column (150 × 4.6 mm, 5 μm; Thermo Scientific, Waltham, MA). The mobile phase was 0.1% formic acid at a flow rate of 1.0 mL/min. The retention time of Gh was 5.5 min. The eluted fractions containing Gh were collected, and their concentration was measured by UV spectra at 230 nm (ε = 3000 M^{-1} cm^{-1}).

Oxazolone and [^{13}C,^{15}N]-Labeled Oxazolone. A mixture of 1.1 mg of riboflavin and 4 mg of dG or the uniformly [^{13}C,^{15}N]-labeled dG in 30 mL water was incubated for 40 min while stirring and irradiated by a 100 W incandescent light bulb positioned at a distance of 6−8 cm. After the incubation, the solution was further stirred at room temperature for overnight. The mixture was applied to a Waters Sep-Pak C_{18} cartridge (Waters), which had been preconditioned by 3 mL of methanol, followed by 3 mL water. The SPE column was washed by 3 mL 2% methanol, and the eluant was purified by HPLC using a Hypercarb column (150 × 4.6 mm, 5 μm, Thermo Scientific). The mobile phase was water with 0.1% formic acid (A) and methanol with 0.1% formic acid (B) as an isocratic mixture of 5% B at a flow rate of 1.0 mL/min. The retention time of Ox was 11 min. The eluted fractions containing Ox were collected, and their concentration was measured by UV spectra at 232 nm (ε = 9000 M^{-1} cm^{-1}).

Treatment of Oligodeoxyribonucleotides with Oxidants. Treatment of double-stranded oligodeoxyribonucleotides (20 μM nucleotide concentration) was performed in 150 mM potassium phosphate and 25 mM sodium bicarbonate (final pH 7.4) using various doses of oxidants. For $ONOOCO_2^-$ treatment, a droplet of peroxynitrite ($ONOO^-$) was added to the sidewall of a tube containing a solution of the oligodeoxyribonucleotide, along with another droplet of an equal volume of 0.3 M HCl to neutralize the NaOH. Following rapid mixing by vortexing, $ONOOCO_2^-$ was generated by rapid reaction of $ONOO^-$ with CO_2. The mixture was incubated for 30 min at 18 °C. For treatment with photoactivated riboflavin, riboflavin was added to the oligodeoxyribonucleotide solution, and the mixture exposed to ultraviolet A light (350 nm) using Rayonet reactor (Southern New England Ultraviolet Company) for 20 min at 4 °C. After treatment, internal standards (11-mer oligodeoxyribonucleotide, 5′-GATCTCGATC-3′) were added to the reaction. The oligodeoxyribonucleotides were then desalted before analysis using LC-MS.

HPLC-QTOF Analysis of Oxidized Oligodeoxyribonucleotides. HPLC was performed using an Agilent series 1200 instrument (Agilent Technologies, Palo Alto, CA), and chromatography was carried out using reversed-phase HPLC with a Hypersil GOLD aQ C18 column (150 mm length × 2.1 mm i.d., 3 μm particle size; Thermo Scientific, Torrance, CA) and a guard cartridge (10 mm length × 2.1 mm i.d., 3 μm particle size). The flow rate was set at 250 μL/min and the column temperature at 25 °C. The solvent system consisted of 10 mM ammonium acetate (A) and acetonitrile (B), with the elution started isocratically at 3% B for 2 min, followed by a linear gradient from 3 to 12% B over 9 min and further to 40% B over 2.5 min, and finally the column was re-equilibrated at 3% B for 10 min. An Agilent 6510 QTOF instrument equipped with an ESI source was employed for both identification and quantification. Oligodeoxyribonucleotide identification was performed by LC-MS/MS in negative ionization mode. Operating parameters were as follows: ESI capillary voltage, 4000 V; gas temperature, 350 °C; drying gas flow, 10 L/min; nebulizer pressure, 50 psi; fragmentor voltage, 200 V; m/z scan range, 900−1200. Relative quantification of the detected oligodeoxyribonucleotides was achieved by normalizing the peak area for each molecular ion against that of the internal standard, to account for variation in injection volume. For mapping of oxidation products within the oligodeoxyribonucleotide, the oxidized oligodeoxyribonucleotide of interest was isolated for CID with a m/z scan range of 300−1600 to generate a fragment ion mass spectrum. The MS/MS fragmentation of an oligodeoxyribonucleotide was predicted using Mongo Oligo Mass Calculator, v2.06 (http://library.med.utah.edu/masspec/mongo.htm).

LC-MS/MS Analysis of Spiroiminodihydantoin, Guanidinohydantoin, and Oxazolone. The dried samples containing Sp, Gh, Ox, and their corresponding isotopomers were dissolved in water. An aliquot of the sample was analyzed by HPLC-ESI-MS/MS using an

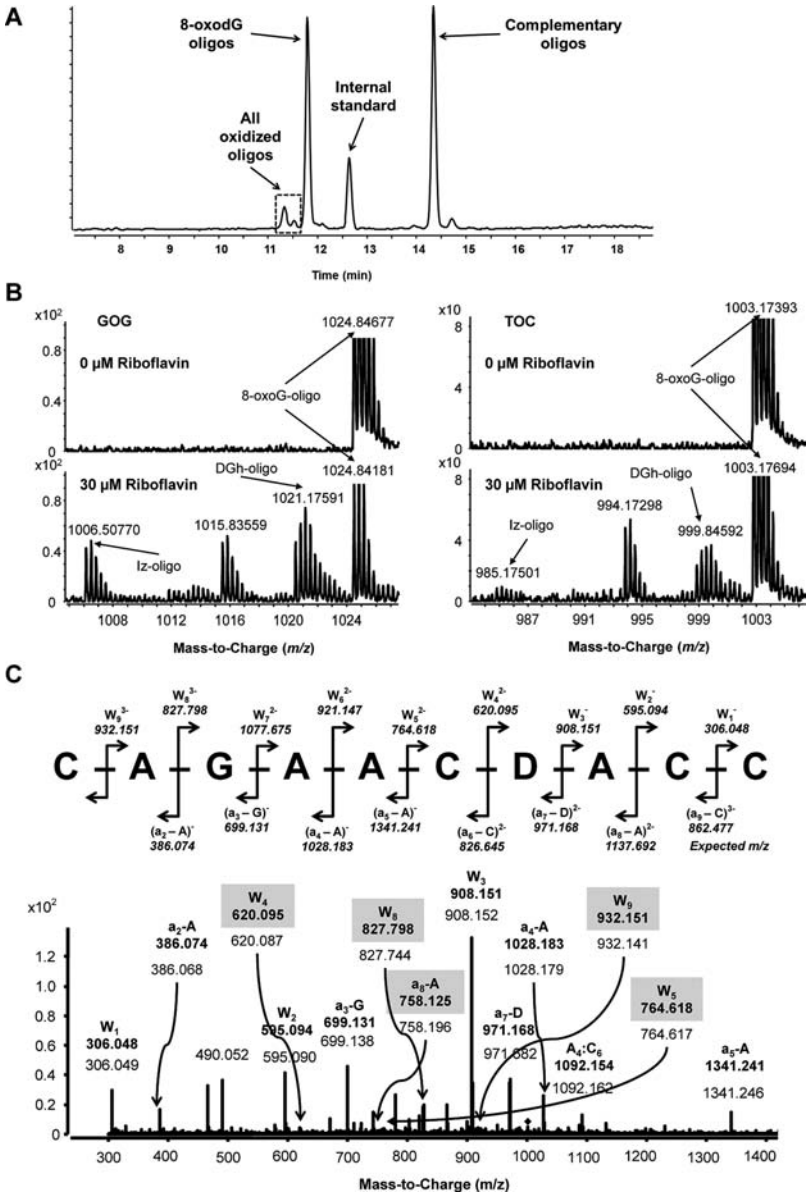

Figure 2. LC-QTOF mass spectrometric analysis of 8-oxodG-oligodeoxyribonucleotide oxidation products. (A) HPLC chromatogram of a reaction mixture containing 8-oxodG oligodeoxyribonucleotide and its oxidation products following photoactivated riboflavin treatment. (B) Negative-ion ESI-MS of a reaction mixture before and after treatment showed the formation of oligodeoxyribonucleotide oxidation products. Oligodeoxyribonucleotides containing GOG and TOC sequences were either untreated (upper panel) or treated with 30 μM of riboflavin (lower panel) in the presence of UVA for 20 min followed by LC-QTOF analysis. (C) Upper panel: predicted fragmentation pattern of DGh-containing oligodeoxyribonucleotide; lower panel: CID analysis of oxidized oligodeoxyribonucleotide. Representative CID fragmentation of a DGh-containing oligodeoxyribonucleotide confirmed the identity and location of the modification.

Agilent 1100 series HPLC system interfaced with an Agilent 6430 triple quadrupole mass spectrometer equipped with a TurboIonSpray source. Samples were resolved on a Hypercarb column (100 × 1.0 mm, 5 μm, Thermo Scientific), using 0.3% formic acid in water (A) and 0.3% formic acid in acetonitrile (B) delivered from 2% to 70% B over 15 min at 20 μL/min. The effluent from the first 5 min from the LC system was diverted to waste to minimize the contamination of the ESI source. A microelectrospray ionization source was employed, and the MS was operated in the positive ion mode. Operating parameters were as follows: ESI capillary voltage, 4000 V; gas temperature, 300 °C; drying gas flow, 8 L/min; nebulizer pressure, 35 psi. Samples were analyzed in multiple reaction monitoring mode, with the following transitions: m/z 300 → 184 and 315 → 194 for Sp and uniformly [^{13}C,^{15}N]-labeled Sp; m/z 274 → 158 and 288 → 167 for Gh and uniformly [^{13}C,^{15}N]-labeled Gh; m/z 247 → 93 and 259 → 87 for Ox and uniformly [^{13}C,^{15}N]-labeled Ox (Figure S1). Calibration curves for the labeled and unlabeled forms of each of the four DNA oxidation products were constructed by plotting the MRM signal ratios between the labeled and unlabeled forms against their corresponding concentration ratios. Quantitation of Sp, Gh, and Ox in each sample was achieved using the MRM signal ratio between analyte of interest and its isotope-labeled internal standard and the response curve.

RESULTS

Method Development and Validation. As illustrated in Figure S2, the strategy for these studies involved (1) synthesis of duplex oligodeoxyribonucleotides containing 8-oxodG in different three-nucleotide sequence contexts; (2) exposure to oxidizing agents; and (3) analysis of damage products by LC-QTOF analysis of intact damaged oligodeoxyribonucleotides. Table 1 shows the set of model oligodeoxyribonucleotide

dx.doi.org/10.1021/ja307525h | J. Am. Chem. Soc. 2012, 134, 18053−18064

Table 2. Mass-to-Charge Ratios of Common Oxidation Products Detected in This Study Following Riboflavin or $ONOOCO_2^-$ Treatment Using GOG Sequence Context As an Example

			m/z^b	
damage product	sequence	mol wt[a]	measured ($n \geq 9$)	calculated
8-oxodG	CAGAA**GOG**CC	3076.558	1024.510 ± 0.005	1024.511
urea	CAGAA**G(Urea)G**CC	2969.546	–	988.840
Iz	CAGAA**G(Iz)G**CC	3021.552	1006.176 ± 0.005	1006.175
Ox	CAGAA**G(Ox)G**CC	3039.562	–	1012.179
OA	CAGAA**G(OA)G**CC	3041.530	1012.834 ± 0.007	1012.835
X[c]	CAGAA**G(X)G**CC	3049.545	1015.507 ± 0.005	–
DGh	CAGAA**G(DGh)G**CC	3064.558	1020.509 ± 0.004	1020.511
Gh	CAGAA**G(Gh)G**CC	3066.573	–	1021.183
Sp	CAGAA**G(Sp)G**CC	3092.553	1029.837 ± 0.006	1029.843
NO_2-DGh	CAGAA**G(NO_2-DGh)G**CC	3109.543	1035.504 ± 0.005	1035.506

[a]Exact molecular weight based upon Mongo Oligo Mass Calculator, v2.06. [b]Based on the ion with −3 charge state in negative ion mode with at least 6 ppm accuracy. [c]An unknown compound that was found during the oxidation of the oligodeoxyribonucleotides.

targets containing 8-oxodG in different three-nucleotide contexts, as described in a recent study of sequence context effects on 8-oxodG reactivity.[22] The length of the oligodeoxyribonucleotides was optimized for the stability of the duplex forms and the need for sufficient mass spectrometric sensitivity and mass accuracy for identification and quantification 8-oxodG oxidation products. The specific sequences represent a subset of all 16 possible trinucleotide sequence contexts of G, and they cover the range of sequence-dependent G IP[8] and the range of reactivities toward oxidation of G and 8-oxodG by $ONOOCO_2^-$ and photoactivated riboflavin.[9,11,13,22] The duplex oligodeoxyribonucleotides all had melting temperatures of 43−52 °C,[22] which ensured duplex structure of the central 8-oxodG sequence context during the oxidation reactions.

The assignment of structures to the m/z values was accomplished by at least two of the following approaches: (1) assignment based on the unique high mass accuracy mass-to-charge (m/z) values of known 8-oxodG damage products; (2) collision-induced dissociation (CID) fragmentation of the oligodeoxyribonucleotides; (3) quantitative analysis of specific 8-oxodG oxidation products by targeted LC-MS/MS analysis of 2-deoxyribonucleosides following enzymatic hydrolysis of the oligodeoxyribonucleotides; and (4) comparison of the kinetics of disappearance of a specific m/z value with published rates of degradation and formation of specific 8-oxodG oxidation products. Following oxidant treatment, the 8-oxodG- or damage-containing strand was resolved from the complementary strand by HPLC (Figure 2A). The identity of each 8-oxodG oxidation product was first determined by comparison of the measured m/z value of the oxidized oligodeoxyribonucleotide to expected m/z values calculated using Mongo Oligo Mass Calculator, v2.06 (http://library.med.utah.edu/masspec/mongo.htm). This is illustrated in Figure 2B, which shows the representative mass spectra of two different oligodeoxyribonucleotides (TOC and GOG) before and after treatment with photoactivated riboflavin. Table 2 shows high mass accuracy m/z values for all of the riboflavin- or $ONOOCO_2^-$-induced oxidation products reproducibly detected in the GOG oligodeoxyribonucleotide, along with a list of anticipated products of 8-oxodG oxidation. For example, the 8-oxodG-containing strand of the GOG oligodeoxyribonucleotide was observed to have an m/z value of 1024.512 ± 0.002 (−3 charge state) compared to a calculated m/z of 1024.511, with a mass accuracy of 1 ppm (Table 1). Following riboflavin oxidation, three new oligodeoxyribonucleotide ions with m/z values of 1006.176 ± 0.005, 1015.507 ± 0.005, and 1020.509 ± 0.004 were consistently observed (Table 2). The first and third ions are assigned to Iz and DGh, respectively, on the basis of their calculated oligodeoxyribonucleotide m/z values, with mass accuracy of 1 and 2 ppm, respectively. The ion with m/z 1015.507 represents a previously unidentified 8-oxodG oxidation product designated "X", which was consistently observed for both $ONOO^-$ and riboflavin treatments. A similar pattern of riboflavin-induced 8-oxodG oxidation is observed in the TOC sequence context, as shown in Figure 2B. While the identification of oxidation products based on high mass accuracy measurements proved to be definitive, the overlapping isotope envelopes of two oxidation products with minimally different m/z values, in some instances, prevented a clear structural assignment for the signal. For example, the m/z value for Gh overlaps with that of DGh (Table S1), making it impossible to quantify Gh. However, because DGh possesses a lower m/z than Gh, we were able to identify and quantify it without interference from Gh using the non-overlapping signals (Table S1). Similarly, Ox and OA both have modestly different m/z values, but a single isotopic signal permits quantification of Ox (Table S2). With $ONOOCO_2^-$ oxidation, however, we are able to quantify OA because Ox abundance was negligible (Table S2). All products reported here had isotope envelopes resolved well enough to extract quantitative information and structural assignment. That oxidant-induced damage in the oligodeoxyribonucleotide constructs occurred only to 8-oxodG was concluded from (1) the significantly greater oxidizability of 8-oxodG compared to G;[14−17] (2) the absence of detectable damage to oligodeoxyribonucleotides lacking 8-oxodG;[22] (3) the localization of damage products to the site of 8-oxodG[22] (see below); and (4) the quantitative loss of 8-oxodG previously observed with these oligodeoxyribonucleotides and oxidants.[22]

With regard to quantitation, while we could not obtain absolute values for the quantities of individual damage products due to the lack of internal standards, we were able to estimate relative amounts of each intact damage-containing oligodeoxyribonucleotide by assuming that the individual oliogdeoxyribonucleotides would be detected with similar efficiency in the mass spectrometer. This is based on the likelihood that the individual base lesions would not significantly affect the efficiency of mass spectrometric detection given the much larger influence of the 10-nucleotide oligo. This assumption was justified by analysis of the signal intensities of identical

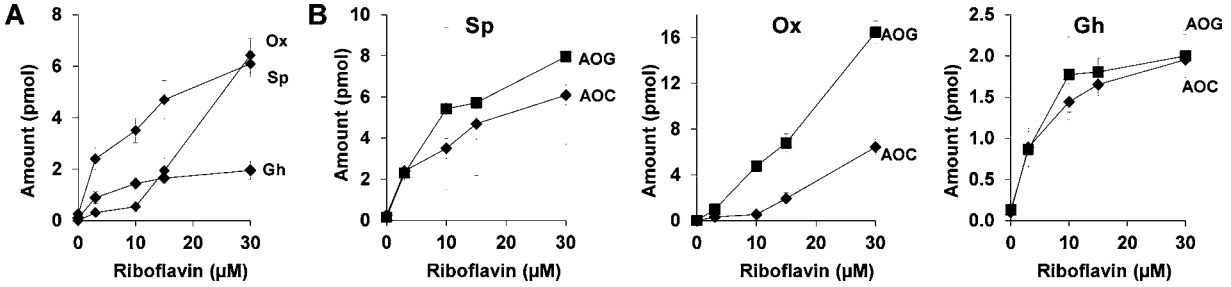

Figure 3. Targeted LC-MS/MS analysis of Sp, Ox, and Gh following photoactivated riboflavin treatment. (A) Measurement of the three nucleosides in AOC oligodeoxyribonucleotides. (B) Comparison of the three nucleosides in two different sequence contexts: AOC and AOG oligodeoxyribonucleotides. Each data point represents mean ± error about the mean for $N = 2$.

quantities of all 16 oligodeoxyribonucleotides, which resulted in a single average signal intensity 4.7 ± 0.5 with a coefficient of variance of 11% (Figure S3). This indicates that we can estimate the relative quantities of oligodeoxyribonucleotides with 11% error, and the resulting signal intensities provide a reasonable estimate of the relative quantity of each damage product for purposes of comparing the effects of different sequence contexts and oxidants.

As mentioned, CID analysis provided information about the location of the 8-oxodG damage product within an oligodeoxyribonucleotide by fragmentation of the phosphodiester backbone of the oligodeoxyribonucleotide, with the pattern of resulting fragments yielding unique patterns reflecting the molecular weight of the damage product. This is illustrated in Figure 2C, in which the upper panel shows the predicted fragmentation pattern of DGh-containing oligodeoxyribonucleotide, and the lower panel shows the CID spectrum of a DGh-containing oligodeoxyribonucleotide in which a parent ion of m/z 1001.844 was used for fragmentation. DGh localized to the fourth position of the oligodeoxyribonucleotide from the 3′-end through identification of two fragment ions with m/z values of 620.095 and 908.151, which correspond to the W_4^{2-} fragment (DACC) and the W_3^- fragment (ACC), respectively (Figure 2C). Examples for Iz, Sp, and NO_2-DGh-oligodeoxyribonucleotides are shown in Figures S4−S6.

The next approach to validation of the QTOF method came from the measurement of Sp, Ox, and Gh products in the AOG and AOC constructs using liquid chromatography coupled triple quadrupole mass spectrometric (LC-QQQ) analysis following digestion of the oxidized oligodeoxyribonucleotides to their 2-deoxynucleoside forms (Figures 3 and S1). As expected, treatment with photoactivated riboflavin caused a dose-dependent increase of Sp, Ox, and Gh in the AOG and AOC oligodeoxyribonucleotides (Figure 3). Furthermore, the relative quantity of riboflavin-induced Ox in the AOG and AOC targets is similar to that for the Ox precursor, Iz, determined by QTOF analysis (seen later with Iz in AOG and AOC in Figure 6B). The 2-deoxyribonucleoside forms of Iz and DGh were not detected in hydrolysates by LC-QQQ analysis, most likely due to the known instability of these products.

Sequence-Dependence of 8-oxodG Oxidation Product Formation. The QTOF-based *in situ* approach was applied to compare the effects of sequence context on the spectrum of 8-oxodG oxidation products caused by two model one-electron oxidants: $ONOOCO_2^-$ and photoactivated riboflavin. With $ONOOCO_2^-$, three major oxidation products were detected in the whole oligodeoxyribonucleotide analysis: DGh, OA, NO_2-DGh (Figure 4). The level of Sp was below the detection limit of the QTOF method for all sequences except AOC, in which maximal formation of Sp occurred between 40 and 200 μM $ONOOCO_2^-$ (Figure 5B). This is consistent with the $ONOOCO_2^-$ concentration dependence of Sp formation observed in previous studies.[23] While the overlapping isotopic signals of DGh and Gh prevented quantification of Gh, there was no detectable signal for Gh following a prolonged (20−24 h) incubation of $ONOOCO_2$-oxidized oligodeoxyribonucleotides in which most of the DGh had decayed into OA. This could be due to levels of Gh-containing oligodeoxyribonucleotides that fall below the detection limit of our QTOF method, which is consistent with the low levels of Gh apparent in the targeted analysis of AOC and AOG oligodeoxynucleotides (Figure 3). Furthermore, DGh was consistently the most abundant oxidation product with $ONOOCO_2^-$ (Figure 4A), with area under the curve (AUC) analyses showing relative abundance in the following order: DGh > OA > NO_2-DGh (Figure 4B). For all $ONOOCO_2^-$ concentrations and in all of the 8-oxodG sequence contexts, there was no apparent effect of sequence context on the relative quantities of the oxidation products (Figure 4A).

The results with photoactivated riboflavin showed several major differences from those with $ONOOCO_2^-$. First, there was a strong sequence dependence in the spectrum of 8-oxodG oxidation products detected with riboflavin: X, DGh, Sp, OA, and Iz (Figure 6A). At riboflavin concentrations ≤30 μM, the unknown oxidation product, X, was generally the most abundant species in all but the AOC sequence context, with significant variation among the relative quantities of the other four products (Figure 6A). At riboflavin concentrations >30 μM, however, DGh emerged as the most abundant species in some sequence contexts (GOG and COA), with Iz matching DGh in AOG and GOG (Figure S7). Surprisingly, exposure of GOG-, COT- and TOC-containing constructs to low riboflavin doses (<15 μM) resulted in relatively high levels of Sp that decreased as a function of increasing riboflavin concentration (Figure 6A). These data indicate that sequence context plays a larger role in determining the spectrum of 8-oxodG oxidation products for photoactivated riboflavin than for $ONOOCO_2^-$.

The role of DNA secondary structure was explored by comparing the relative quantities of riboflavin-mediated 8-oxodG oxidation products in single- and double-stranded oligodeoxyribonucleotides. As shown in Figure S8, 8-oxodG was more reactive toward oxidation in single-stranded substrates in which there was generally higher levels of DGh, OA, and Sp; Iz formation was less dependent on secondary structure.

Kinetics of Product Formation and Transformation. To explore the kinetics of transformation of 8-oxodG oxidation products *in situ* in DNA and to corroborate the identities of

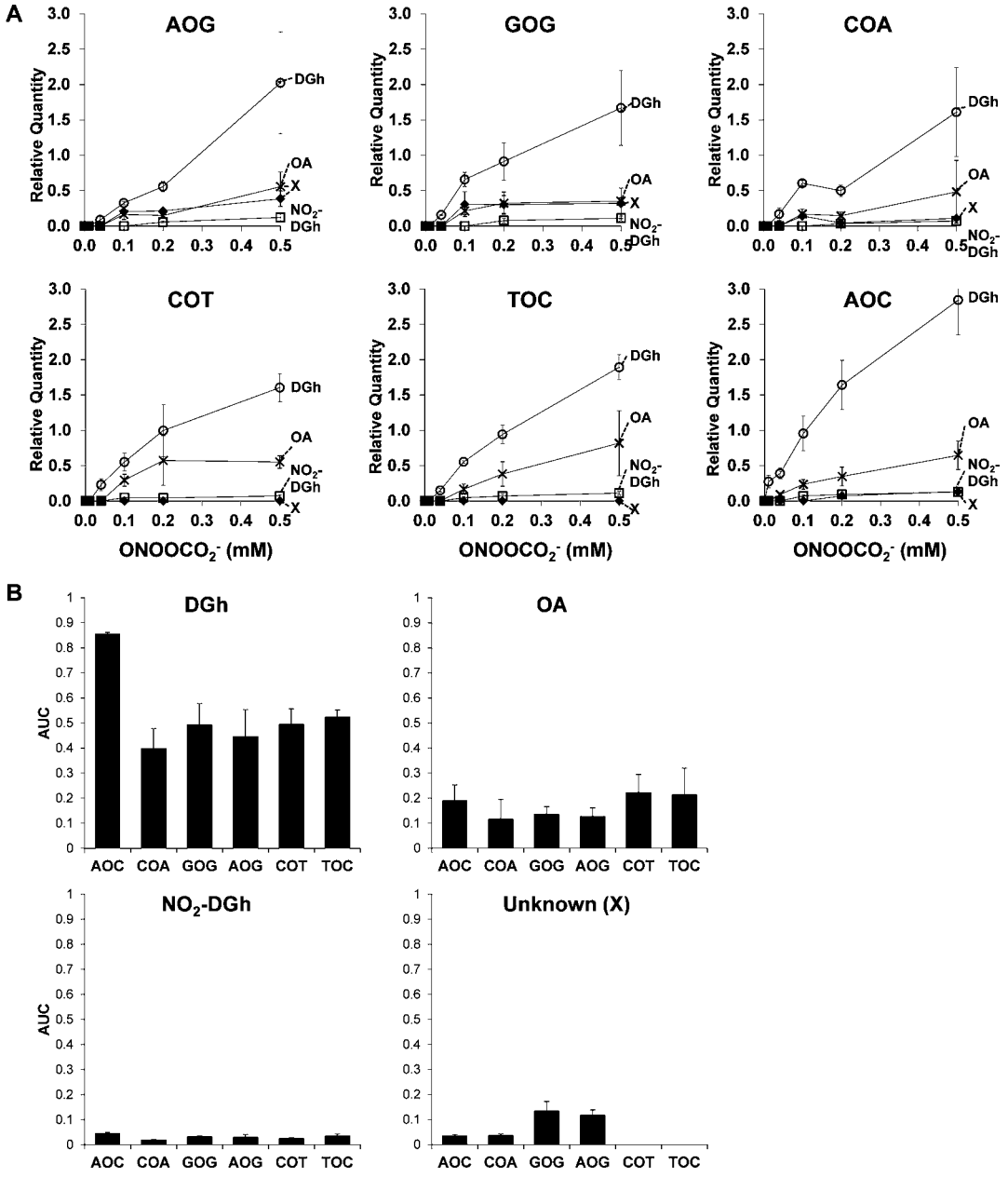

Figure 4. Sequence dependence study of 8-oxodG oxidation by $ONOOCO_2^-$. (A) LC-QTOF analysis of the relative abundance of three major oxidation products, DGh, OA, and NO_2-DGh oligodeoxyribonucleotides, following $ONOOCO_2^-$ treatment reveals no apparent effect of sequence context on the relative quantities of the oxidation products. Relative quantification of the detected oligodeoxyribonucleotides was achieved by normalizing the peak area for each molecular ion against that of the internal standard. Each data point represents mean ± standard deviation calculated for $N = 3$. (B) Formation of 8-oxodG products expressed as AUC; AUC values for $ONOOCO_2^-$ dose−response curves were calculated by the trapezoidal method for each replicate data set, with mean ± standard deviation for $N = 3$.

individual products, the QTOF analytical method was applied to analyze the spectrum of riboflavin-induced oxidation products as a function of time in the COA and GOG oligodeoxyribonucleotides. As shown in Figure 7, levels of 8-oxodG and Sp remained relatively constant in the 24 h following oxidant treatment, as expected for the two chemically stable products. However, levels of Iz, DGh, and NO_2-DGh decreased over time, while OA increased (Figure 7). The loss of Iz occurred with a first-order rate constant of 0.2 ± 0.05 h^{-1} ($t_{1/2}$ = 2.9 ± 0.6 h; 37 °C), which is similar to the 2.5 h half-life (37 °C) of the 2-deoxynucleoside form of Iz.[24] Similarly, decay of DGh and NO_2-DGh occurred with first-order rate constants of 0.09 ± 0.04 h^{-1} ($t_{1/2}$ = 7 ± 3 h) and 0.17 ± 0.05 h^{-1} ($t_{1/2}$ = 4 ± 1 h), respectively, which is consistent with published DGh half-life of ∼5 h[25] and with our observation of the kinetics of formation of OA, the degradation product of both DGh and NO_2-DGh (k = 0.08 ± 0.02 h^{-1}; $t_{1/2}$ = 9 ± 2 h; Figures 1 and 7).[18−20]

Characterization of a Novel 8-oxodG Oxidation Product. Riboflavin-induced photooxidation of 8-oxodG in the various oligodeoxyribonucleotides resulted in the formation of a previously unidentified product (X). This new product has a mass that is 27.009 Da lower than that of 8-oxodG, with a monoisotopic mass of approximately 140.03 for the base and 256.08 for the 2-deoxynucleoside (Figure 8A), which is consistent with a putative molecular formula of $C_9H_{12}N_4O_5$

dx.doi.org/10.1021/ja307525h | J. Am. Chem. Soc. 2012, 134, 18053−18064

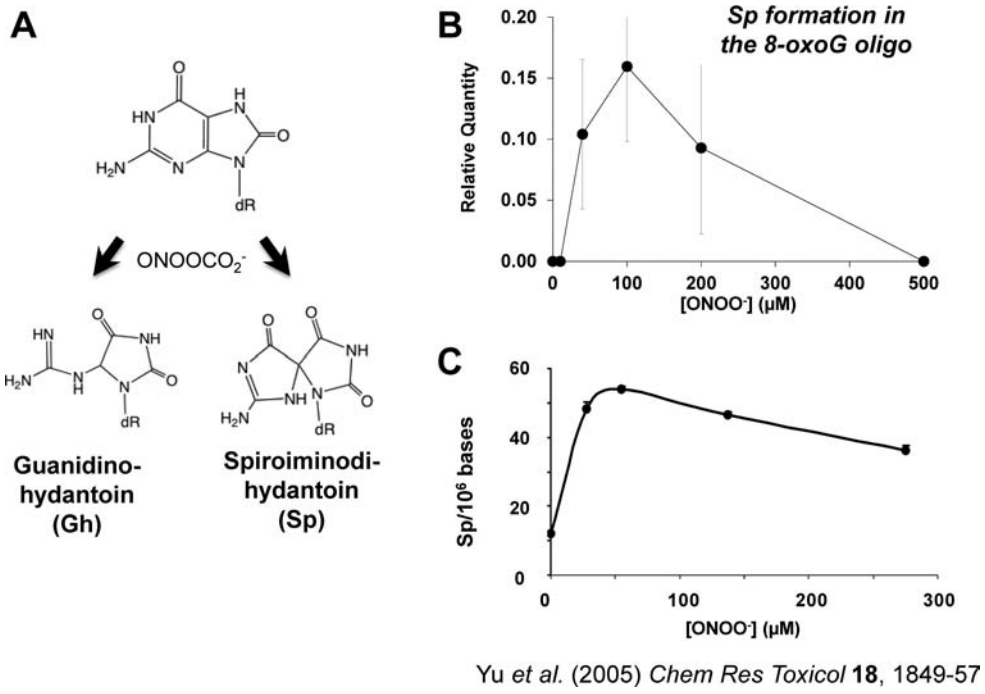

Figure 5. Formation of Sp during $ONOOCO_2^-$ treatment. (A) Scheme illustrating the reaction of $ONOOCO_2^-$ with 8-oxodG to form Sp and Gh. (B) The AOC construct was treated with varying concentrations of $ONOOCO_2^-$, and Sp was quantified in the intact oligodeoxynucleotide using the QTOF approach, as described in Experimental Methods. Each data point represents mean ± standard deviation for $N = 3$. (C) A plot of Sp formation as a function of $ONOOCO_2^-$ concentration, using data taken from ref 23.

and thus the loss of HCN from 8-oxodG. While X was observed in all sequence contexts with riboflavin-mediated photooxidation (Figure 6A), with significant sequence-dependent formation (Figure 8B), it formed only in double-stranded oligodeoxyribonucleotides and not in single-stranded constructs (Figure 8C). Furthermore, X was unstable, with complete disappearance by 2 h at 37 °C (Figure 8D) and a half-life of ∼5 h at 25 °C (Figure 8E). As a result, we were not able to characterize X by analysis of a 2-deoxyribonucleoside. However, CID fragmentation analysis performed on freshly oxidized oligodeoxynucleotides confirmed the molecular weight of the 2-deoxynucleoside form as 256.08 Da and its location at the fourth position from the 3′ end of the oligodeoxyribonucleotide (Figure S9). Definitive structural characterization awaits further study.

■ DISCUSSION

Progress in our understanding of the mechanisms of mutagenesis is hampered by our inability to predict which products will arise at a site of DNA damage or, more specifically, how the local environment influences the course of chemical reactions that eventually lead to a stable product. While advances in DNA charge transfer chemistry allow us to predict that guanine oxidation will occur most frequently in sequence contexts that confer the lowest ionization potential (e.g., runs of guanine; ref 9), we cannot predict which of the dozen different guanine oxidation products will arise at the final damage site. We approached this problem by developing a high-resolution and high mass accuracy mass spectrometry method for *in situ* identification and quantification of the spectrum of damage products that arise at a specific site in an oligodeoxyribonucleotide and applied the method to analyze the effects of local DNA sequence on the oxidation of 8-oxodG. This well-studied guanine oxidation product is susceptible to further oxidation to yield a diverse set of stable species (Figure 1) (4, 17, 18), with several of these species recently identified *in vivo*.[26−28] The identities of oxidation products in the 10-mer oligodeoxyribonucleotide substrates were verified in several ways, including molecular weight matching, CID analysis to localize and characterize the products, quantitative comparisons with targeted LC-MS/MS analysis of specific products, and comparisons of molecular transformation kinetics. Furthermore, the analysis of intact oligodeoxyribonucleotides provided an opportunity for estimating the relative quantities of the various damage products, with an approximately 10% detector response variation for the different oligodeoxyribonucleotides. In this way, we were able to identify and quantify many known 8-oxodG oxidation products (Table 2), including DGh, NO_2-DGh, OA, Iz, and Sp, and the approach led to the discovery of what appears to be a novel and relatively abundant damage product. Furthermore, given the short time frame between the oxidation event and subsequent analysis of damage products, we were able to observe the *in situ* transformation of relatively unstable species and to define the kinetics of the transformation in the setting of a duplex DNA structure.

A survey of the range of damage products arising in the six 8-oxodG sequence contexts revealed several observations. First, DGh was consistently observed to be one of the most abundant 8-oxodG oxidation products for both $ONOOCO_2^-$ and riboflavin (Figures 4 and 6). The analogous NO_2-DGh was, as expected, only detected with $ONOOCO_2^-$ and was the least abundant product with this oxidant. Both NO_2-DGh and DGh are relatively unstable species ($t_{1/2} \sim 7$ h; *vide infra*; refs 29 and 30) and undergo transformation to OA (Figure 1), which we were able to monitor *in situ* using the LC-QTOF approach. Further validation for this approach is derived from the relative proportions of the 8-oxodG oxidation products arising with the bolus dosing of $ONOOCO_2^-$ used in the present studies (i.e.,

dx.doi.org/10.1021/ja307525h | J. Am. Chem. Soc. 2012, 134, 18053−18064

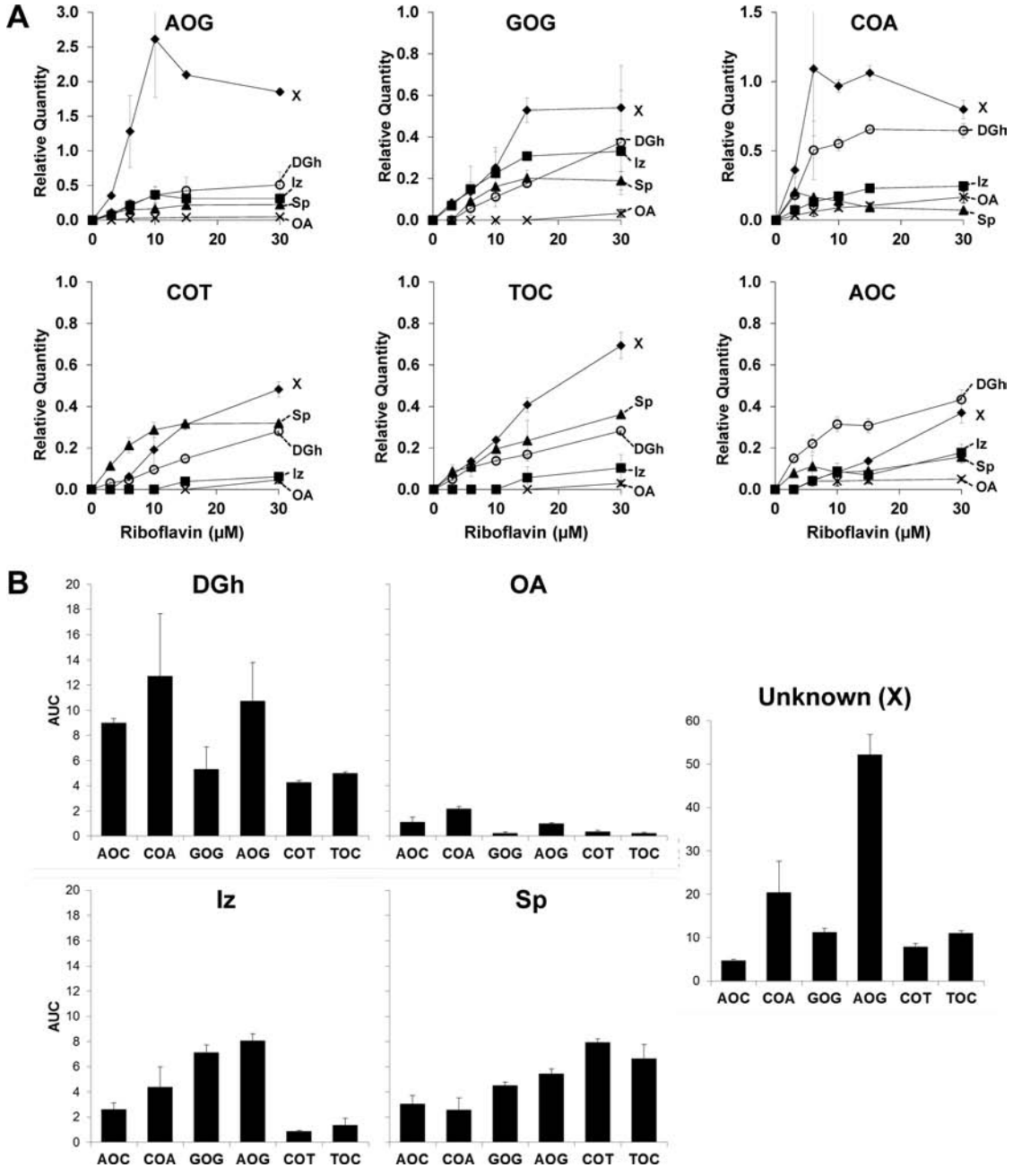

Figure 6. Sequence-dependent oxidation of 8-oxodG-containing oligodeoxyribonucleotides by photoactivated riboflavin. (A) LC-QTOF was used to quantify the relative abundance of oligodeoxyribonucleotides containing individual 8-oxodG oxidation products. Relative quantification of the detected oligodeoxyribonucleotides was achieved by normalizing the peak area for each molecular ion against that of the internal standard. Each data point represents mean ± standard deviation calculated for $N = 3$. (B) Sequence-dependent formation of 8-oxodG products expressed as AUC. AUC values for photoactivated riboflavin dose−response curves were calculated by the trapezoidal method for each data set, with mean and standard deviation calculated for $N = 3$. Note that AOG and COA have a different Y-axis scale.

high levels of DGh and OA and low levels of Sp), which are consistent with previous studies.[20]

A second important observation was the discovery of a novel 8-oxodG oxidation product (X) with both $ONOOCO_2^-$ and riboflavin-mediated photooxidation (Figures 4, 6, and 8). While it is a minor product with $ONOOCO_2^-$ (Figure 4), it is among the major products arising with riboflavin-mediated photooxidation of 8-oxodG (Figures 6, 8). Its instability, with a half-life of ∼5 h at 37 °C, obviated structural definition and likely accounts for the fact that it has not been described previously in the well-studied chemistry of G and 8-oxoG oxidation.[20]

With regard to the influence of DNA secondary structure on damage chemistry, sequence context has been shown to have significant effects on the reactivity of G and 8-oxodG toward oxidation.[9,11,13,22,31] However, there is limited information about the influence of neighboring bases on the pathways that determines the spectrum of final oxidation products.[11,13] Our comparative analysis of 8-oxodG oxidation in the six oligodeoxyribonucleotide constructs revealed strong agent-specific effects of sequence context on the spectrum of products. While $ONOOCO_2^-$ showed strong sequence context effects for both reactivity of G and the proportions of G

dx.doi.org/10.1021/ja307525h | J. Am. Chem. Soc. 2012, 134, 18053−18064

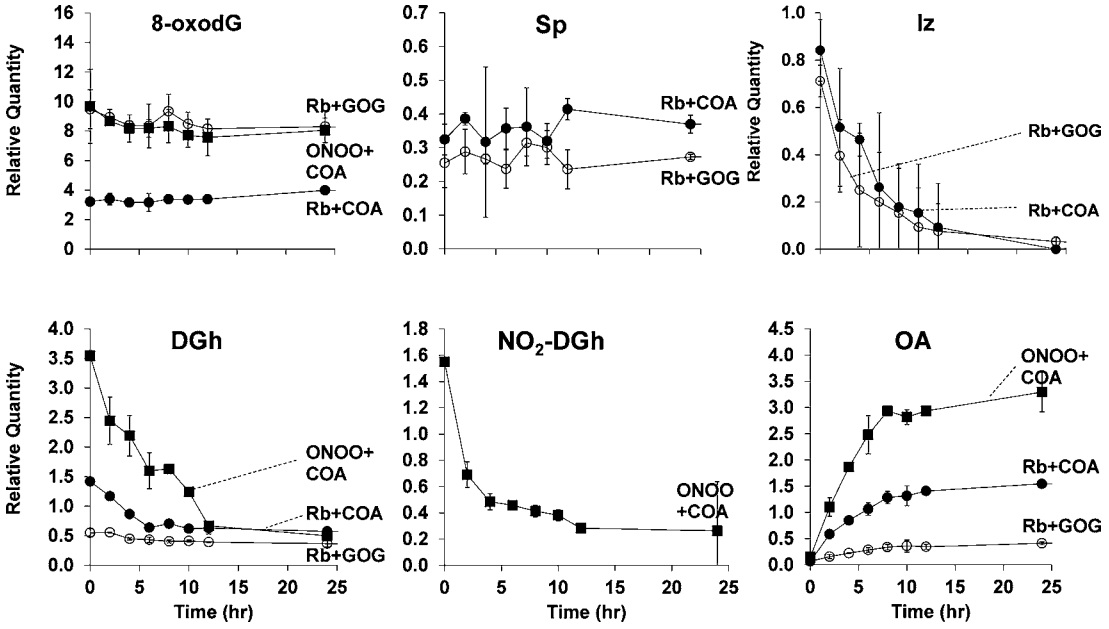

Figure 7. Kinetic analysis of oxidation products after treatment with $ONOOCO_2^-$ and photoactivated riboflavin. COA and GOG oligodeoxyribonucleotides were treated with $ONOOCO_2^-$ or photoactivated riboflavin as described in the Experimental Methods. Following incubation at 37 °C for 0−24 h, the oligodeoxyribonucleotides were analyzed by LC-QTOF to define the stability of the oxidation products. Relative quantification of the detected oligodeoxyribonucleotides was achieved by normalizing the peak area for each molecular ion against that of the internal standard. Each data point represents mean ± error about the mean for $N = 2$.

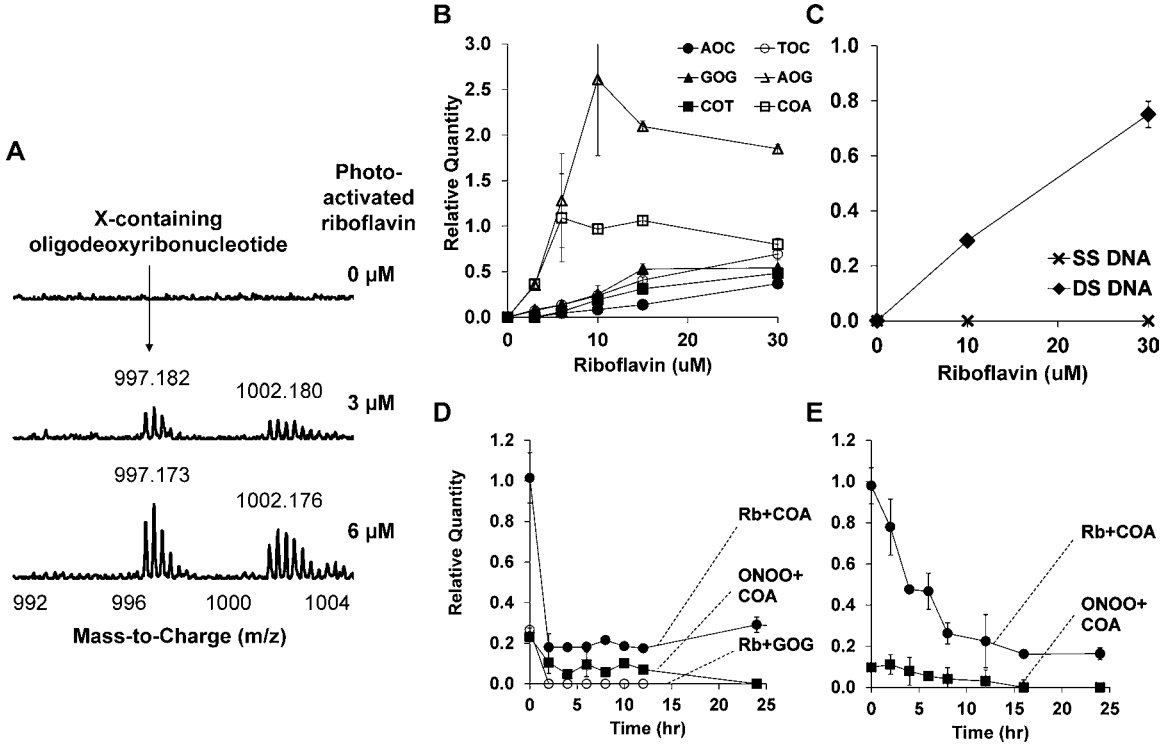

Figure 8. Characterization of the novel 8-oxodG oxidation product, X. (A) Mass spectra for 8-oxodG-containing oligodeoxyribonucleotides following treatment with 0, 3, or 6 μM photoactivated riboflavin. (B) Comparison of the relative quantity of X in all six sequence contexts. (C) Comparison of the relative quantity of X in single- and double-stranded forms of AOG. Each data point represents mean ± standard deviation for $N = 3$. (D,E) Stability of X in oligodeoxyribonucleotides at 37 °C (D) and 25 °C (E). Relative quantification of the X-containing oligodeoxyribonucleotides was achieved by normalizing the peak area for each molecular ion against that of the internal standard. Each data point represents mean ± error about the mean for $N = 2$.

oxidation products (measured indirectly as alkali- and enzymatically labile sites; ref 11), the relative quantities of $ONOOCO_2^-$-induced 8-oxodG oxidation products were not affected by sequence context (Figure 4), which parallels our recent observation of a lack of sequence context effect on the reactivity of 8-oxodG with $ONOOCO_2^-$.[22]

dx.doi.org/10.1021/ja307525h | J. Am. Chem. Soc. 2012, 134, 18053−18064

For riboflavin-induced photooxidation, however, there was a broader spectrum of 8-oxodG oxidation products, and the quantities of these products varied widely among the six sequences (Figure 6). The higher levels of Sp for riboflavin, as compared to $ONOOCO_2^-$, are consistent with previously observed oxidation of 8-oxo-7,8-dihydroguanosine by riboflavin-mediated photooxidation causing three major products: Sp > Gh > Iz.[32] The sequence dependence of 8-oxodG oxidation by riboflavin stands in contrast to our previous observation of minimal sequence effects on the spectrum of riboflavin-induced G oxidation products (again measured indirectly as alkali- and enzymatically labile sites; ref 13). There is no apparent correlation between the sequence dependence of 8-oxodG reactivity with riboflavin, which we recently quantified,[22] and the relative quantities of the various 8-oxodG oxidation products (Figure 6), while correlations between the ease of oxidation of 8-oxodG and the product spectrum await calculations of the sequence-dependent ionization potentials for 8-oxodG, as determined for G.[9]

The observation of strong sequence context effects on the final chemistry of DNA oxidation complicates our understanding of the mechanistic basis for both mutation frequency and mutational spectra caused by DNA damage *in vivo*. It is not surprising that local sequence-determined DNA structural factors, such as solvent exposure, electrostatics, and the proximity of nucleophilic exocyclic atoms on nucleobases, would affect the course of chemical reactions involved in DNA oxidation. However, there are also significant sequence-dependent variations in rates of DNA repair of individual DNA lesions, with slowly repaired locations showing strong correlation with mutation hotspots (e.g., refs 33−35). The combination of sequence-dependent DNA oxidation product spectra and sequence-dependent repair efficiency thus complicates the interpretation of mutational spectra derived from cells and tissues subjected to endogous oxidative stresses. Furthermore, evidence points to DNA base damage repair rates in mammalian cells with half-lives on the order of hours (e.g., refs 36−38), which is similar to the observed kinetics of transformation of several 8-oxodG oxidation products, such as DGh, NO_2-DGh, Iz, OA, and X. As a complicating factor in DNA repair, a scenario can be envisioned in which the primary lesion, such as DGh, initiates a specific DNA repair response only to transform into another lesion, OA and subsequently urea in the case of DGh, that requires a different repair mechanism.

CONCLUSION

In summary, we have developed an analytical method to identify and quantify DNA oxidation products *in situ* in intact oligodeoxyribonucleotides. This approach revealed significant effects of both sequence context and the identity of the oxidant on the spectrum of DNA oxidation products as well as the discovery of a novel DNA oxidation product and transformation of DNA lesions on a biologically relevant time scale. The results have implications for understanding the chemistry of DNA oxidation and the biological response to the damage.

ASSOCIATED CONTENT

Supporting Information

Two tables of mass spectrometric data and nine figures showing the experiment workflow, mass spectrometric data, and results from experimental control studies. This material is available free of charge via the Internet at http://pubs.acs.org.

AUTHOR INFORMATION

Corresponding Author

pcdedon@mit.edu; kslim@mit.edu

Present Addresses

[⊥]Singapore-MIT Alliance on Research and Technology, Singapore

[∥]Department of Chemistry, Hong Kong University of Science & Technology Clear Water Bay, Kowloon, Hong Kong

Notes

The authors declare no competing financial interest.

ACKNOWLEDGMENTS

We thank Drs. Nicholas E. Geacintov and Vladimir Shafirovich for insightful discussions and critical review of the manuscript. This work was supported by grants from the National Cancer Institute (CA026731 and CA110261). Mass spectrometry studies were performed in the Bioanalytical Facilities Core of the MIT Center for Environmental Health Science, which is funded by Center grant ES002109 from the National Institute of Environmental Health Sciences.

REFERENCES

(1) Mattes, W. B.; Hartley, J. A.; Kohn, K. W. *Nucleic Acids Res.* **1986**, *14*, 2971−2987.

(2) Matter, B.; Guza, R.; Zhao, J.; Li, Z. Z.; Jones, R.; Tretyakova, N. *Chem. Res. Toxicol.* **2007**, *20*, 1379−1387.

(3) Denissenko, M. F.; Pao, A.; Tang, M.-s.; Pfeifer, G. P. *Science* **1996**, *274*, 430−432.

(4) Oleykowski, C. A.; Mayernik, J. A.; Lim, S. E.; Groopman, J. D.; Grossman, L.; Wogan, G. N.; Yeung, A. T. *J. Biol. Chem.* **1993**, *268*, 7990−8002.

(5) Giese, B. *Annu. Rev. Biochem.* **2002**, *71*, 51−70.

(6) Schuster, G. B. *Acc. Chem. Res.* **2000**, *33*, 253−260.

(7) Ito, K.; Inoue, S.; Yamamoto, K.; Kawanishi, S. *J. Biol. Chem.* **1993**, *268*, 13221−13227.

(8) Sugiyama, H.; Saito, I. *J. Am. Chem. Soc.* **1996**, *118*, 7063−7068.

(9) Saito, I.; Nakamura, T.; Nakatani, K.; Yoshioka, Y.; Yamaguchi, K.; Sugiyama, H. *J. Am. Chem. Soc.* **1998**, *120*, 12686−12687.

(10) Saito, I.; Takayama, M.; Sugiyama, H.; Nakatani, K. *J. Am. Chem. Soc.* **1995**, *117*, 6406−6407.

(11) Margolin, Y.; Cloutier, J. F.; Shafirovich, V.; Geacintov, N. E.; Dedon, P. C. *Nat. Chem. Biol.* **2006**, *2*, 365−366.

(12) Lee, Y. A.; Durandin, A.; Dedon, P. C.; Geacintov, N. E.; Shafirovich, V. *J. Phys. Chem. B* **2008**, *112*, 1834−1844.

(13) Margolin, Y.; Shafirovich, V.; Geacintov, N. E.; DeMott, M. S.; Dedon, P. C. *J. Biol. Chem.* **2008**, *283*, 35569−35578.

(14) Sheu, C.; Foote, C. S. *J. Am. Chem. Soc.* **1995**, *117*, 6439−6442.

(15) Uppu, R. M.; Cueto, R.; Squadrito, G. L.; Salgo, M. G.; Pryor, W. A. *Free Radical Biol. Med.* **1996**, *21*, 407−411.

(16) Steenken, S.; Jovanovic, S. V. *J. Am. Chem. Soc.* **1997**, *119*, 617−618.

(17) Steenken, S.; Jovanovic, S. V.; Bietti, M.; Bernhard, K. *J. Am. Chem. Soc.* **2000**, *122*, 2373−2374.

(18) Cadet, J.; Douki, T.; Ravanat, J. L. *Acc. Chem. Res.* **2008**, *41*, 1075−1083.

(19) Burrows, C. J.; Muller, J. G.; Kornyushyna, O.; Luo, W.; Duarte, V.; Leipold, M. D.; David, S. S. *Environ. Health Perspect.* **2002**, *110* (Suppl 5), 713−717.

(20) Niles, J. C.; Wishnok, J. S.; Tannenbaum, S. R. *Nitric Oxide* **2006**, *14*, 109−121.

(21) Spassky, A.; Angelov, D. *Biochemistry* **1997**, *36*, 6571−6576.

(22) Lim, K. S.; Taghizadeh, K.; Wishnok, J. S.; Babu, I. R.; Shafirovich, V.; Geacintov, N. E.; Dedon, P. C. *Chem. Res. Toxicol.* **2012**, *25*, 366−373.

(23) Yu, H.; Venkatarangan, L.; Wishnok, J. S.; Tannenbaum, S. R. *Chem. Res. Toxicol.* **2005**, *18*, 1849−1857.

(24) Raoul, S.; Bergert, M.; Buchko, G. W.; Joshi, P. C.; Morin, B.; Weinfeld, M.; Cadet, J. *J. Chem. Soc., Perkin Trans. 2* **1996**, *1996*, 371−381.
(25) Chworos, A.; Seguy, C.; Pratviel, G.; Meunier, B. *Chem. Res. Toxicol.* **2002**, *15*, 1643−1651.
(26) Matter, B.; Malejka-Giganti, D.; Csallany, A. S.; Tretyakova, N. *Nucleic Acids Res.* **2006**, *34*, 5449−5460.
(27) Hailer, M. K.; Slade, P. G.; Martin, B. D.; Rosenquist, T. A.; Sugden, K. D. *DNA Repair* **2005**, *4*, 41−50.
(28) Mangerich, A.; Knutson, C. G.; Parry, N. M.; Muthupalani, S.; Ye, W.; Prestwich, E.; Cui, L.; McFaline, J. L.; Mobley, M.; Ge, Z.; Taghizadeh, K.; Wishnok, J. S.; Wogan, G. N.; Fox, J. G.; Tannenbaum, S. R.; Dedon, P. C. *Proc. Natl. Acad. Sci. U.S.A.* **2012**, *109*, E1820−E1829.
(29) Duarte, V.; Gasparutto, D.; Yamaguchi, L. F.; Ravanat, J. L.; Martinez, G. R.; Medeiros, M. H. G.; Di Mascio, P.; Cadet, J. *J. Am. Chem. Soc.* **2000**, *122*, 12622−12628.
(30) Chworos, A.; Coppel, Y.; Dubey, I.; Pratviel, G.; Meunier, B. *J. Am. Chem. Soc.* **2001**, *123*, 5867−5877.
(31) Hickerson, R. P.; Prat, F.; Muller, J. G.; Foote, C. S.; Burrows, C. J. *J. Am. Chem. Soc.* **1999**, *121*, 9423−9428.
(32) Luo, W.; Muller, J. G.; Burrows, C. J. *Org. Lett.* **2001**, *3*, 2801−2804.
(33) Tommasi, S.; Oxyzoglou, A. B.; Pfeifer, G. P. *Nucleic Acids Res.* **2000**, *28*, 3991−3998.
(34) Tornaletti, S.; Pfeifer, G. P. *Science* **1994**, *263*, 1436−1438.
(35) Tu, Y.; Bates, S.; Pfeifer, G. P. *J. Biol. Chem.* **1997**, *272*, 20747−20755.
(36) Smith, S. A.; Engelward, B. P. *Nucleic Acids Res.* **2000**, *28*, 3294−3300.
(37) Ye, N.; Holmquist, G. P.; O'Connor, T. R. *J. Mol. Biol.* **1998**, *284*, 269−285.
(38) Klungland, A.; Rosewell, I.; Hollenbach, S.; Larsen, E.; Daly, G.; Epe, B.; Seeberg, E.; Lindahl, T.; Barnes, D. E. *Proc. Natl. Acad. Sci. U.S.A.* **1999**, *96*, 13300−13305.